



UNIVERSITY OF LEEDS

This is a repository copy of *Highly sensitive Fourier-transform coherent anti-Stokes Raman scattering spectroscopy via genetic algorithm pulse shaping.*

White Rose Research Online URL for this paper:

<https://eprints.whiterose.ac.uk/222078/>

Version: Accepted Version

---

**Article:**

Lindley, M., Gala de Pablo, J. [orcid.org/0000-0003-0557-9632](https://orcid.org/0000-0003-0557-9632), Kinegawa, R. et al. (2 more authors) (2021) Highly sensitive Fourier-transform coherent anti-Stokes Raman scattering spectroscopy via genetic algorithm pulse shaping. *Optics Letters*, 46 (17). pp. 4320-4323. ISSN 0146-9592

<https://doi.org/10.1364/ol.434054>

---

© 2021 Optical Society of America. One print or electronic copy may be made for personal use only. Systematic reproduction and distribution, duplication of any material in this paper for a fee or for commercial purposes, or modifications of the content of this paper are prohibited.

**Reuse**

Items deposited in White Rose Research Online are protected by copyright, with all rights reserved unless indicated otherwise. They may be downloaded and/or printed for private study, or other acts as permitted by national copyright laws. The publisher or other rights holders may allow further reproduction and re-use of the full text version. This is indicated by the licence information on the White Rose Research Online record for the item.

**Takedown**

If you consider content in White Rose Research Online to be in breach of UK law, please notify us by emailing [eprints@whiterose.ac.uk](mailto:eprints@whiterose.ac.uk) including the URL of the record and the reason for the withdrawal request.



[eprints@whiterose.ac.uk](mailto:eprints@whiterose.ac.uk)  
<https://eprints.whiterose.ac.uk/>

# Highly sensitive Fourier-transform coherent anti-Stokes Raman scattering spectroscopy via genetic algorithm pulse shaping

MATTHEW LINDLEY,<sup>1</sup> JULIA GALA DE PABLO,<sup>1</sup> RYO KINEGAWA,<sup>1</sup> KOTARO HIRAMATSU,<sup>1,2,3,\*</sup> AND KEISUKE GODA<sup>1,4,5,\*</sup>

<sup>1</sup>Department of Chemistry, The University of Tokyo, Tokyo 113-0033, Japan

<sup>2</sup>Research Centre for Spectrochemistry, The University of Tokyo, Tokyo 113-0033, Japan

<sup>3</sup>PRESTO, Japan Science and Technology Agency, Saitama 332-0012, Japan

<sup>4</sup>Institute of Technological Sciences, Wuhan University, Hubei 430072, China

<sup>5</sup>Department of Bioengineering, University of California, Los Angeles, California 90095, USA

\*Corresponding author: \*hiramatsu@chem.s.u-tokyo.ac.jp (K.H.); goda@chem.s.u-tokyo.ac.jp (K.G.)

Received XX Month XXXX; revised XX Month, XXXX; accepted XX Month XXXX; posted XX Month XXXX (Doc. ID XXXXX); published XX Month XXXX

---

**We report highly sensitive Fourier-transform coherent anti-Stokes Raman scattering spectroscopy enabled by genetic algorithm (GA) pulse shaping for adaptive dispersion compensation. We show that the non-resonant four-wave mixing signal from water can be used as a fitness indicator for successful GA training. This method allows GA adaptation to sample measurement conditions and offers significantly improved performance compared to training using second harmonic generation from a nonlinear crystal in place of the sample. Results include a 3× improvement to peak signal to noise ratio for 2-propanol measurement, as well as a 10× improvement to peak intensities from the high-throughput measurement of polystyrene microbeads under flow.**

---

Fourier-transform coherent anti-Stokes Raman scattering (FT-CARS) spectroscopy [1–3] is a time-domain Raman spectroscopic method, where molecular vibrations are excited and interrogated with ultrashort pulses. FT-CARS spectroscopy is distinguished from other coherent Raman methods, such as frequency-domain CARS and stimulated Raman scattering spectroscopy, by its capability to produce broadband, background-free Raman spectra. The spectral acquisition rate of FT-CARS, which is determined by the scanning rate of the delay between ultrashort pump-probe pulses, can be higher than a few tens of kHz using a rapid mechanical scanner or dual-comb techniques [4,5]. FT-CARS spectral bandwidth is determined by its optical pulse bandwidth, resulting in Raman spectra spanning more than 3,000 cm<sup>-1</sup> demonstrated with sub-10 fs pulses [6,7]. Initially developed with an eye towards microscopy [8–10], the progression of FT-CARS spectroscopy to the ultrafast regime has opened the technique to high-throughput applications such as flow cytometry, where it has been used to study metabolic dynamics in large microalgal populations with single-cell resolution [11,12].

Unfortunately, the sensitivity of FT-CARS spectroscopy, like other methods for coherent Raman scattering spectroscopy, is often limited to the low millimolar range,

depending on the analyte [13,14]. Sensitivity enhancement via pulse shaping has been explored in time-domain Raman spectroscopy using spectral focusing [15–17], non-resonant background (NRB) suppression [18,19], and signal enhancement by pulse compression [20,21]. In the case of FT-CARS, spectral focusing sacrifices the mixed-analyte detection ability of its broadband measurement while background suppression is already accomplished via careful selection of the Fourier-transform region. The remaining approach, time-domain Raman spectroscopy, has been demonstrated in previous CARS works using spectrally resolved second harmonic generation (SHG) to analytically characterize the spectral phase of the pulse. These efforts produced transform-limited or near-transform limited pulses in the nonlinear optical crystals they employed [20,21]. However, in applications with a high-NA objective, such as microscopy or flow cytometry, pulse shaping with a replacement nonlinear medium does not always offer optimal pulses for sample measurement because the temporal and spatial profiles of the pulse in the sample can differ significantly from its profiles in the replacement medium [22]. Additionally, implementing spectrally resolved SHG detection can complicate the experimental setup.

Genetic algorithm (GA) pulse shaping offers an adaptive approach to dispersion compensation in nonlinear optical systems, where the GA is used to search the space of phase compensation solutions [23,24]. GA progression towards an optimized solution can be judged experimentally with a spectrally resolved measurement, or naively with a signal-intensity-based approach. While previous demonstrations typically used SHG from a nonlinear crystal or four-wave-mixing (FWM) from graphene [25] at the sample position, the adaptive nature of GA pulse shaping implies it can function without sample replacement provided that a suitable nonlinear signal can be achieved under the spectrometer's normal configuration.

Here we report highly sensitive FT-CARS spectroscopy with a high-NA objective enabled by GA pulse shaping using a spatial light modulator (SLM). Importantly, we show that the non-resonant FWM intensity signal from water in the spectrometer's normal sample container can serve as a fitness feedback mechanism. This allows GA-based pulse compensation with no modification to the system's normal optical configuration, both simplifying the setup and ensuring dispersion compensation addresses the system as used during sample measurement. Using our method, we demonstrate a more than 3× improvement in signal-to-noise ratio (SNR) from a pure solvent (2-propanol), allowing us to resolve weaker peaks otherwise lost to noise with only chirped mirror pulse compression. We also demonstrate a ~10× improvement in peak intensity from polymer microbeads measured under high-throughput flow-through measurement conditions at ~360 beads/s.

A schematic of our FT-CARS spectrometer and the GA pulse shaper is shown in Figure 1A. Briefly, the system consists of a Ti:Sapphire pulsed laser (pulse width 16 fs, Coherent, Vitara T-HP) as the light source, an SLM pulse shaper and chirped mirrors (Thorlabs, DCMP175) for dispersion compensation, a rapid-scan pulse pair generator for interferometry, and a PC for signal digitization (AlazarTech, ATS9440) and analysis. In a flow cytometer configuration, we placed a microfluidic chip with integrated acoustic focusing to flow particles or cells at the optical focus between a paired objective and condenser (Olympus, LCPLANN50X0.65IR). We used LabVIEW (National Instruments, version 2016) for real-time spectral analysis during pulse shaping and Igor Pro (WaveMetrics, version 8) for post-processing of experimental data. The pulse shaper was constructed from a dispersive prism (Thorlabs, PS859), a cylindrical concave mirror (Thorlabs, CCM400P01), and SLM (Santec, SLM200) configured in a retroreflective 4-f configuration with the SLM at the Fourier plane.

We wrote the pulse shaping GA in LabVIEW based on previous work [26]. Our algorithm began by seeding 50 random genes, each composed of 192 values. These values set the optical phase displacement by the SLM pixels, with each value assigned to 10 binned pixels across the 1,920 horizontal pixels of the device (pixels were vertically uniform). The pulse shape for each gene was tested and assigned a score by a fitness feedback mechanism. The top 20% of genes from each generation were cross-bred and mutated to create 50 genes for the next generation. To

prevent a decrease in fitness, a copy of the top-scoring gene was passed unchanged to the new generation as well.

To measure an FT-CARS spectrum, the pulse pair generator split each incoming pulse into a pair of pulses and scanned intra-pair delay from ~50 fs to ~1.8 ps. The first pulse (pump) of each pair drove coherent vibration in the sample and the second (probe) scattered from it. The

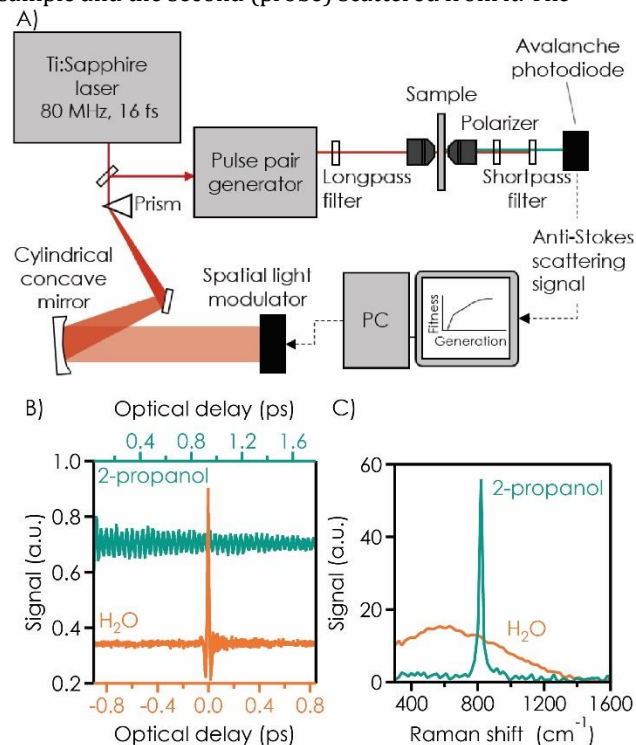


Fig. 1. Schematic and example spectra. A) Schematic of FT-CARS with integrated 4-f SLM pulse shaper. B) Example of time-domain signal acquisitions. Normally the pulse-pair overlap region (optical delay < 0.05 ps) is moved outside of the acquisition region to remove non-resonant background signal, as shown for 2-propanol. This non-resonant signal region can be seen by the large intensity in the pulse overlap region in the corresponding H<sub>2</sub>O interferogram. C) Raman shift spectra recovered from the Fourier-transform of the traces in A. The 2-propanol trace shows a vibrationally resonant peak with low background. The H<sub>2</sub>O trace shows the broad spectrum produced by non-resonant wave mixing at the pulse-pair overlap region.

probability for this scattering to produce anti-Stokes photons was modulated in time by the vibrational wave packet, so that anti-Stokes scattering intensity measurements iterated across increasing delay mapped the vibration in the time domain. A full scan took 41.7  $\mu$ s. Signal detection was enhanced by a long-pass filter (Thorlabs, FELH0750), used to create a sharp spectral edge along the blue side of each pulse before the sample, and a short-pass filter (Thorlabs, FESH0750), used to remove unshifted probe light after the sample. The signal was digitized to create a time-domain interferogram.

The measurement of 2-propanol is shown in Figure 1B. The Fourier transform (FT) of this interferogram produced the Raman spectrum shown in Figure 1C. A strong non-resonant anti-Stokes signal during pump-probe overlap (around 0 fs) can be seen in the interferogram for water in Figure 1B and its FT spectrum is shown in Figure 1C. This broad, bandwidth-spanning FWM spectrum is referred to as NRB in CARS literature, and is a significant source of spectral distortion. Normally in FT-CARS, this pulse overlap region is windowed out of the FT to entirely avoid NRB distortion in the recovered spectra. However, the non-linear, non-resonant nature of this phenomenon allows it to function as a Raman-mode-agnostic reporter of pulse intensity during GA pulse shaping.

We detected the non-resonant FWM signal with two different methods for pulse shaping feedback. The first, which we call "Signal 1," measured the spectral intensity of the FT-CARS-recovered NRB spectrum. This signal was measured as the spectral geometric mean from 300 – 1,600  $\text{cm}^{-1}$  averaged across  $\sim 2$  ms of acquisition. The second, which we call "Signal 2," consisted of photo intensity at the anti-Stokes scattering detector averaged across 2 ms. While the first method is limited to systems able to recover a CARS spectrum, the second is applicable to systems outside the CARS discipline by the inclusion of a shortpass filter before the photodetector. Given the nature of FWM, we expected a cubic power dependence from both Signal 1 and Signal 2, but with measurement found a 2.9 and 2.4 power dependence, respectively. This suggested that the anti-Stokes scattering in the system included a non-FWM optical process that transited the shortpass filter but fell outside the FT-CARS spectral region. Nevertheless, the nonlinear nature of both phenomena allowed them to be used as fitness feedback signals for GA pulse shaping aimed at maximizing pulse intensity. For comparison, we also performed GA pulse shaping with SHG as a fitness feedback mechanism after replacing the sample container with a  $\beta$ -barium borate (BBO) crystal (reported as "SHG" in the data). To compare results to performance without the pulse shaper (reported as "Control" in the data), we removed the pulse shaper from the beamline and optimized the number of chirped mirrors bounces at  $-5600$  fs<sup>2</sup> based on FT-CARS peak intensity from 2-propanol (increased from the value of  $-4550$  fs<sup>2</sup> used during pulse shaping).

Pulse shaping with each fitness mechanism was continued for several hundred generations until fitness improvement flattened. Each generation took  $\sim 30$  seconds to complete. To directly compare the results of the different pulse shaping methods, we loaded profiles from every 50<sup>th</sup> generation of the methods onto the SLM and measured the FT-CARS NRB spectrum of water. A fitness score was then assigned based on the area under the NRB curve, with scores shown in Figure 2A. The final SLM pattern for each method is shown in Figure 2B. The spectrally dispersed light was located on the central third of the SLM face. While both profiles trained against the H<sub>2</sub>O in the flow cell show a similar structure, we note that the SHG profile trained with the BBO at the sample position is distinctly different. This suggests a significant difference in index of refraction between the media. Spectra of 2-propanol taken from the control

condition and the final Signal 1 pulse shaping profile are compared in Figure 2C. Both spectra are an average of 100 acquisitions (4.2 ms of measurement) and have been normalized to peak height. The improvement from pulse shaping is apparent as a reduction in baseline noise and the appearance of peaks at 490 and 957  $\text{cm}^{-1}$ . We calculated the SNR (mean intensity divided by standard deviation) for these peaks for the final pulse profile from both methods and the control, shown in the Figure 2B inset. The best pulse shaping

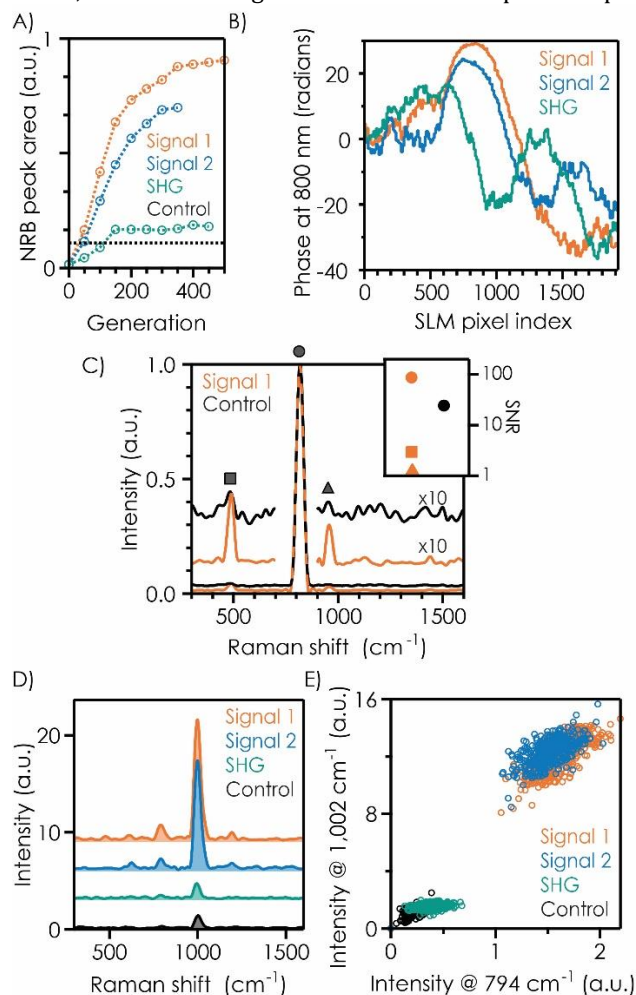


Fig. 2. Pulse shaping results. A) GA fitness progression mapped as Signal 1 spectral area at every 50<sup>th</sup> generation of pulse shaping. B) Final SLM pattern for each method. C) Spectra from 2-propanol measured with the final Signal pulse shaping profile and the control, normalized to peak height. Inset) Corresponding signal to noise ratios (average / standard deviation) at the three peak positions indicated by markers in C (490  $\text{cm}^{-1}$ , 817  $\text{cm}^{-1}$ , and 906  $\text{cm}^{-1}$ ). Unshown markers have SNR < 1. D) Single-bead spectra taken with the final SLM profile for each pulse shaping experiment, offset from zero for clarity. E) Scatter plot of peak intensities for PS beads under flow. N =  $\sim 400$  events for each group.

Result, which yielded a 3 $\times$  increase in SNR over the control. While this study produced the best result with Signal 1 as the

GA feedback mechanism, in principle both Signal 1 and Signal 2 fitness scores should converge given enough time.

To demonstrate signal improvement for a high-throughput FT-CARS spectroscopy application, we performed particle measurement under flow-through conditions to simulate Raman flow cytometry. Specifically, we measured 6- $\mu\text{m}$  polystyrene (PS) beads at a flow rate of 4 cm/s with five spectral acquisitions per event. An event is defined as the triggering of measurement by the passage of a bead, bead-cluster, or debris. For triggering, we used the rising edge of the forward-scattering signal. Throughput was  $360 \pm 16$  events/s, counted as event triggers across 1 s for three repeats. Analysis of forward scattering data allowed removal of events triggered by an out-of-focus bead or a bead cluster. We did this to ensure that signal fluctuations due to poor acoustic focusing or multiple-bead events had a minimal effect on results. Single event Raman spectra can be seen in Figure 2D. All spectra in Figure 2 were interpolated with a spline to determine peak intensities. A scatter plot of these peak intensities is shown in Figure 2E. Overall, pulse shaping with both Signal 1 and Signal 2 produced a  $10\times$  increase in Raman peak intensity over the control method, as shown by the single bead spectra and peak intensity scatterplot. This improvement should directly translate to higher sample throughput in flow cytometry applications with biological samples, which are typically throughput-limited by their much weaker signals. The SHG-based pulse shaping profile, optimized in a BBO crystal, did not produce results better than the control for measurement in a flow cytometry chip. Though we believe this was largely due to refractive index differences between the crystal and flow chip, we note that our simple method was unable to extract the spectral phase of the pulse. This phase information is required to claim that the pulse profile in the BBO was fully optimized before returning to the flow chip.

These results indicate that the non-resonant FWM signal from water works well as a feedback mechanism for GA pulse compression in FT-CARS spectroscopy. The use of water as a nonlinear optical medium simplified the pulse shaping setup and minimized potential differences in system dispersion between GA training and sample measurement. While our method lacked the pulse characterization provided by more complex analytical approaches (and thereby any claims of reaching the transform limit), it provided a robust and easy method for increasing signal (SNR by  $3\times$  and peak intensities by  $10\times$ ) with minimal modification to the system. This improvement can translate to higher sample throughput and the detection of lower concentration analytes or weaker Raman modes. Planned applications for our improved system include Raman-activated cell sorting [27]. While this demonstration utilized an FT-CARS spectrometer, the use of FWM as a pulse shaping feedback mechanism can in principle easily be extended to other nonlinear spectrometers with femtosecond pulsed laser sources.

**Funding.** This work was supported by KISTEC, JST PRESTO (JPMJPR1878), JSPS Core-to-Core Program, JSPS Grant-in-Aid for Young Scientists (20K15227), Grant-in-Aid for JSPS Fellows (19F19805 & 21J15001), Nakatani Foundation, White Rock Foundation, Ogasawara Foundation.

**Disclosures.** K.G. is a shareholder of CYBO and Cupido

**Data availability.** Data underlying the results presented in this paper are not publicly available at this time but may be obtained from the authors upon reasonable request.

**Code availability.** Code used for analysis of the results presented in this paper may be obtained from the authors upon reasonable request.

## References

1. H. Graener and A. Laubereau, *Opt. Commun.* **54**, 141 (1985).
2. A. Volkmer, L. D. Book, and X. S. Xie, *Appl. Phys. Lett.* **80**, 1505 (2002).
3. J. P. Ogilvie, E. Beaufort, A. Alexandrou, and M. Joffe, *Opt. Lett.* **31**, 480 (2006).
4. M. Tamamitsu, Y. Sakaki, T. Nakamura, G. K. Podagatlapalli, T. Ideguchi, and K. Goda, *Vib. Spectrosc.* **91**, 163 (2017).
5. R. Kameyama, S. Takizawa, K. Hiramatsu, and K. Goda, *ACS Photonics* **8**, 975 (2020).
6. N. Coluccelli, E. Vicentini, A. Gambetta, C. R. Howle, K. McEwan, P. Laporta, and G. Galzerano, *Opt. Express* **26**, 18855 (2018).
7. K. Hashimoto, J. Omachi, and T. Ideguchi, *Opt. Express* **26**, 14307 (2018).
8. M. Cui, M. Joffe, J. Skodack, and J. P. Ogilvie, *Opt. Express* **14**, 8448 (2006).
9. A. S. Duarte, C. Schnedermann, and P. Kukura, *Sci. Rep.* **6**, 37516 (2016).
10. R. Kinoshita, K. Hiramatsu, K. Hashimoto, V. R. Badarla, T. Ideguchi, and K. Goda, *J. Raman Spectrosc.* **50**, 1141 (2019).
11. K. Hiramatsu, T. Ideguchi, Y. Yonamine, S. Lee, Y. Luo, K. Hashimoto, T. Ito, M. Hase, J.-W. Park, Y. Kasai, S. Sakuma, T. Hayakawa, F. Arai, Y. Hoshino, and K. Goda, *Sci. Adv.* **5**, eaau0241 (2019).
12. K. Hiramatsu, K. Yamada, M. Lindley, K. Suzuki, and K. Goda, *Biomed. Opt. Express* **11**, 1752 (2020).
13. C. H. Camp Jr and M. T. Cicerone, *Nat. Photonics* **9**, 295 (2015).
14. R. C. Prince and E. O. Potma, *J. Biomed. Opt.* **26**, 060601 (2021).
15. B. von Vacano and M. Motzkus, *Opt. Commun.* **264**, 488 (2006).
16. J. Konradi, A. Scaria, V. Namboodiri, and A. Materny, *J. Raman Spectrosc.* **38**, 1006 (2007).
17. S. Zhang, L. Zhang, X. Zhang, L. Ding, G. Chen, Z. Sun, and Z. Wang, *Chem. Phys. Lett.* **433**, 416 (2007).
18. D. Oron, N. Dudovich, and Y. Silberberg, *Phys. Rev. Lett.* **90**, 213902 (2003).
19. S. O. Konorov, M. W. Blades, and R. F. B. Turner, *Appl. Spectrosc.* **64**, 767 (2010).
20. H. Kuramochi, S. Takeuchi, and T. Tahara, *Rev. Sci. Instrum.* **87**, 043107 (2016).
21. R. Viljoen, P. Neethling, D. Spangenberg, A. Heidt, H.-M. Frey, T. Feurer, and E. Rohwer, *J. Opt. Soc. Am. B* **37**, A259 (2020).
22. M. Pawłowska, S. Goetz, C. Dreher, M. Wurdack, E. Krauss, G. Razinkas, P. Geisler, B. Hecht, and T. Brixner, *Opt. Express* **22**, 31496 (2014).
23. T. Baumert, T. Brixner, V. Seyfried, M. Strehle, and G. Gerber, *Applied Physics B: Lasers and Optics* **65**, 779 (1997).
24. A. M. Weiner, *Opt. Commun.* **284**, 3669 (2011).
25. R. Ciesielski, A. Comin, M. Handloser, K. Donkers, G. Piredda, A. Lombardo, A. C. Ferrari, and A. Hartschuh, *Nano Lett.* **15**, 4968 (2015).
26. F. G. Omenetto, B. P. Luce, and A. J. Taylor, *J. Opt. Soc. Am. B* **16**, 2005 (1999).
27. N. Nitta, T. Iino, A. Isozaki, M. Yamagishi, Y. Kitahama, S. Sakuma, Y. Suzuki, H. Tezuka, M. Oikawa, F. Arai, T. Asai, D. Deng, H. Fukuzawa, M. Hase, T. Hasunuma, T. Hayakawa, K. Hiraki, K. Hiramatsu, Y. Hoshino, M. Inaba, Y. Inoue, T. Ito, M. Kajikawa, H. Karakawa, Y. Kasai, Y. Kato, H. Kobayashi, C. Lei, S. Matsusaka, H. Mikami, A. Nakagawa, K. Numata, T. Ota, T. Sekiya, K. Shiba, Y. Shirasaki, N. Suzuki, S. Tanaka, S. Ueno, H. Watarai, T. Yamano, M. Yazawa, Y. Yonamine, D. Di Carlo, Y.

## References (with titles)

1. H. Graener and A. Laubereau, "High resolution Fourier transform Raman spectroscopy with ultrashort laser pulses," *Opt. Commun.* **54**(3), 141–146 (1985).
2. A. Volkmer, L. D. Book, and X. S. Xie, "Time-resolved coherent anti-Stokes Raman scattering microscopy: Imaging based on Raman free induction decay," *Appl. Phys. Lett.* **80**(9), 1505–1507 (2002).
3. J. P. Ogilvie, E. Beaurepaire, A. Alexandrou, and M. Joffre, "Fourier-transform coherent anti-Stokes Raman scattering microscopy," *Opt. Lett.* **31**(4), 480–482 (2006).
4. M. Tamamitsu, Y. Sakaki, T. Nakamura, G. K. Podagatlapalli, T. Ideguchi, and K. Goda, "Ultrafast broadband Fourier-transform CARS spectroscopy at 50,000 spectra/s enabled by a scanning Fourier-domain delay line," *Vib. Spectrosc.* **91**, 163–169 (2017).
5. R. Kameyama, S. Takizawa, K. Hiramatsu, and K. Goda, "Dual-comb coherent Raman spectroscopy with near 100% duty cycle," *ACS Photonics* **8**(4), 975–981 (2020).
6. N. Coluccelli, E. Vicentini, A. Gambetta, C. R. Howle, K. Mcewan, P. Laporta, and G. Galzerano, "Broadband Fourier-transform coherent Raman spectroscopy with an ytterbium fiber laser," *Opt. Express* **26**(15), 18855–18862 (2018).
7. K. Hashimoto, J. Omachi, and T. Ideguchi, "Ultra-broadband rapid-scan Fourier-transform CARS spectroscopy with sub-10-fs optical pulses," *Opt. Express* **26**(11), 14307–14314 (2018).
8. M. Cui, M. Joffre, J. Skodack, and J. P. Ogilvie, "Interferometric Fourier transform coherent anti-Stokes Raman scattering," *Opt. Express* **14**(18), 8448–8458 (2006).
9. A. S. Duarte, C. Schnedermann, and P. Kukura, "Wide-field detected Fourier transform CARS microscopy," *Sci. Rep.* **6**(1), 37516 (2016).
10. R. Kinogawa, K. Hiramatsu, K. Hashimoto, V. R. Badarla, T. Ideguchi, and K. Goda, "High-speed broadband Fourier-transform coherent anti-stokes Raman scattering spectral microscopy," *J. Raman Spectrosc.* **50**(8), 1141–1146 (2019).
11. K. Hiramatsu, T. Ideguchi, Y. Yonamine, S. Lee, Y. Luo, K. Hashimoto, T. Ito, M. Hase, J.-W. Park, Y. Kasai, S. Sakuma, T. Hayakawa, F. Arai, Y. Hoshino, and K. Goda, "High-throughput label-free molecular fingerprinting flow cytometry," *Sci. Adv.* **5**(1), eaau0241 (2019).
12. K. Hiramatsu, K. Yamada, M. Lindley, K. Suzuki, and K. Goda, "Large-scale label-free single-cell analysis of paramylon in *Euglena gracilis* by high-throughput broadband Raman flow cytometry," *Biomed. Opt. Express* **11**(4), 1752–1759 (2020).
13. C. H. Camp Jr and M. T. Cicerone, "Chemically sensitive bioimaging with coherent Raman scattering," *Nat. Photonics* **9**(5), 295–305 (2015).
14. R. C. Prince and E. O. Potma, "Coherent Raman scattering microscopy: capable solution in search of a larger audience," *J. Biomed. Opt.* **26**(06), 060601 (2021).
15. B. von Vacano and M. Motzkus, "Time-resolved two color single-beam CARS employing supercontinuum and femtosecond pulse shaping," *Opt. Commun.* **264**(2), 488–493 (2006).
16. J. Konradi, A. Scaria, V. Namboodiri, and A. Materny, "Application of feedback-controlled pulse shaping for control of CARS spectra: the role of phase and amplitude modulation," *J. Raman Spectrosc.* **38**(8), 1006–1021 (2007).
17. S. Zhang, L. Zhang, X. Zhang, L. Ding, G. Chen, Z. Sun, and Z. Wang, "Selective excitation of CARS by adaptive pulse shaping based on genetic algorithm," *Chem. Phys. Lett.* **433**(4), 416–421 (2007).
18. D. Oron, N. Dudovich, and Y. Silberberg, "Femtosecond phase-and-polarization control for background-free coherent anti-Stokes Raman spectroscopy," *Phys. Rev. Lett.* **90**(21), 213902 (2003).
19. S. O. Konorov, M. W. Blades, and R. F. B. Turner, "Lorentzian amplitude and phase pulse shaping for nonresonant background suppression and enhanced spectral resolution in coherent anti-Stokes Raman scattering spectroscopy and microscopy," *Appl. Spectrosc.* **64**(7), 767–774 (2010).
20. H. Kuramochi, S. Takeuchi, and T. Tahara, "Femtosecond time-resolved impulsive stimulated Raman spectroscopy using sub-7-fs pulses: Apparatus and applications," *Rev. Sci. Instrum.* **87**(4), 043107 (2016).
21. R. Viljoen, P. Neethling, D. Spangenberg, A. Heidt, H.-M. Frey, T. Feurer, and E. Rohwer, "Implementation of temporal ptychography algorithm, i 2 PIE, for improved single-beam coherent anti-Stokes Raman scattering measurements," *J. Opt. Soc. Am. B* **37**(11), A259 (2020).
22. M. Pawłowska, S. Goetz, C. Dreher, M. Wurdack, E. Krauss, G. Razinkas, P. Geisler, B. Hecht, and T. Brixner, "Shaping and spatiotemporal characterization of sub-10-fs pulses focused by a high-NA objective," *Opt. Express* **22**(25), 31496–31510 (2014).
23. T. Baumert, T. Brixner, V. Seyfried, M. Strehle, and G. Gerber, "Femtosecond pulse shaping by an evolutionary algorithm with feedback," *Applied Physics B: Lasers and Optics* **65**(6), 779–782 (1997).
24. A. M. Weiner, "Ultrafast optical pulse shaping: A tutorial review," *Opt. Commun.* **284**(15), 3669–3692 (2011).
25. R. Ciesielski, A. Comin, M. Handloser, K. Donkers, G. Piredda, A. Lombardo, A. C. Ferrari, and A. Hartschuh, "Graphene Near-Degenerate Four-Wave Mixing for Phase Characterization of Broadband Pulses in Ultrafast Microscopy," *Nano Lett.* **15**(8), 4968–4972 (2015).
26. F. G. Omenetto, B. P. Luce, and A. J. Taylor, "Genetic algorithm pulse shaping for optimum femtosecond propagation in optical fibers," *J. Opt. Soc. Am. B* **16**(11), 2005–2009 (1999).
27. N. Nitta, T. Iino, A. Isozaki, M. Yamagishi, Y. Kitahama, S. Sakuma, Y. Suzuki, H. Tezuka, M. Oikawa, F. Arai, T. Asai, D. Deng, H. Fukuzawa, M. Hase, T. Hasunuma, T. Hayakawa, K. Hiraki, K. Hiramatsu, Y. Hoshino, M. Inaba, Y. Inoue, T. Ito, M. Kajikawa, H. Karakawa, Y. Kasai, Y. Kato, H. Kobayashi, C. Lei, S. Matsusaka, H. Mikami, A. Nakagawa, K. Numata, T. Ota, T. Sekiya, K. Shiba, Y. Shirasaki, N. Suzuki, S. Tanaka, S. Ueno, H. Watarai, T. Yamano, M. Yazawa, Y. Yonamine, D. Di Carlo, Y. Hosokawa, S. Uemura, T. Sugimura, Y. Ozeki, and K. Goda, "Raman image-activated cell sorting," *Nat. Commun.* **11**(1), 3452 (2020).